Dynamic column loss analysis of reinforced concrete flat slabs

J.M. Russell[a,*], J.S. Owen[b], I. Hajirasouliha[c]

[a]*School of Engineering, University of Warwick, UK*
[b]*Faculty of Engineering, The University of Nottingham, UK*
[c]*Department of Civil and Structural Engineering, The University of Sheffield, UK*

Abstract

The sudden column loss idealisation is a useful design tool to assess structures for progressive collapse. As such an event is a dynamic problem, suitable account must be taken of these effects. This can either be achieved by a full dynamic analysis of the structure or a simplified static approach, with correction factors for the dynamic influence. This study aims to investigate the response of Reinforced Concrete (RC) flat slab structures after a column loss using experimentally validated Finite Element (FE) models. The nonlinear dynamic response of a structure after such an event is considered, including the redistribution of loads and displacement profile. These results are then compared to equivalent static cases in order to determine the Dynamic Amplification Factor (DAF). For the range of structures considered, the DAF was calculated as between 1.39 and 1.62 for displacements, with lower factors associated with a higher nonlinear response or slower column removal. Additionally, the shear forces in remaining columns may exceed 200% of their fully supported condition, with a different associated DAF. The effects of

*Corresponding author.
Email address: j.russell.3@warwick.ac.uk (J.M. Russell)

increasing the tensile strength of concrete due to high strain rates are also considered. Typical Dynamic Increase Factors (DIFs) based on the strain rates were up to 1.23, however, this only applied for a short time period, and in a limited area. Therefore, such effects do not significantly influence the response.
Keywords: Progressive Collapse, Column Loss, RC Flat Slab, Dynamic Amplification

---

1. Introduction

Progressive collapse has been shown to be an important issue in the design of structures after the collapses of a number of buildings including Ronan Point in 1968 and the Murrah Federal Building bombing in 1995. One design approach is to use a scenario-independent analysis, such as a sudden column loss, which idealises the possible event by removing a support and analysing the response of the remaining structure and ensuring it has suitable alternative load paths. This approach is adopted in a number of international codes (see for example [1–3]). While a static loading simulation is often used in practice, such an event is in reality a dynamic problem. Previous studies have considered this issue, demonstrating that a structure may be statically safe but dynamically unsafe [4]. The inertial effects involved create an amplification of the forces applied to surrounding elements, often called the Dynamic Amplification Factor (DAF), defined as ratio of the peak dynamic value of a parameter to the static case. Most commonly displacements are used to calculate this value. Other parameters, such as forces, may give different DAFs. The magnitude of the amplification factor has been shown to vary depending on structural form and the extent of damage [5–10]. The majority of the research on this topic has been focused on response of

beam structures [11–14], however, it is expected that flat slab construction will behave differently due to the two dimensional redistribution of forces that can result in different mechanical response [15, 16]. Additionally the potential for brittle failures such as punching shear, increase the risk of progressive collapse [17, 18]. The DAF for flat slabs construction has been experimentally measured at between 1.13-1.23 [19], however this is based on limited data and parameters and requires further investigation. Furthermore, Lui et al.'s [20] important work on the response of flat slab structures to progressive collapse highlights that such structures can be highly susceptible to extreme events and that further studies are needed.

Additionally, different rates of loading affects the modulus of elasticity, peak compressive and tensile strengths, and post peak behaviour of engineering materials. Typically, for RC structures, the most critical of these is the increase in yield stress for the reinforcement and cracking stress for concrete, which is modelled by a Dynamic Increase Factor (DIF). This may reduce the extent of damage during a dynamic event. Malvar and Ross [21] conducted a comprehensive review on concrete tensile tests at various strain-rates, which indicated that the tensile DIF is dependant on the material properties of the concrete, as well as the rate of loading. In their experimental investigation on beams under a sudden column loss, Yu et al. [10] measured strain rates of between 10^{-2} to 10^{-1}/s, and suggested that this only gives a small increase in material strength and can be conservatively ignored.

In this study the dynamic effects of a column loss event on RC flat slab structures are investigated for different geometric and material parameters. Numerical models are first validated against experimental tests on scaled substructures and then a range of dynamic column loss events are simulated. Subsequently, the re-

sults are compared to equivalent static cases to determine DAFs corresponding to each case. Additionally, the role of strain rate on the tensile strength of concrete is considered to determine the significance of such effects for progressive collapse. The results provide valuable confirmation of previous studies as well adding to the understanding of the behaviour of RC flat slab structures, which can lead to more efficient designs.

2. Description of the finite element model

To assess the response of a concrete flat slab structure to a column loss event, detailed Finite Element (FE) models were created and analysed using Abaqus/explicit [22]. An explicit code was used because it is particularly suited to nonlinear transient dynamics problems. First, the FE model of a slab was validated against experimental tests on RC slabs, then a structural model was developed to assess the response of typical flat slab structures for progressive collapse.

Solid 8 node brick elements (C3N8R) with reduced integration were used to model the concrete sections, which also allow inclusion of geometric nonlinearity effects such as the formation of compressive membranes which can increase the stiffness of continuous slabs due to the in-plane constraint [15, 23]. A mesh sensitivity study was conducted to identify the optimum number and size of the concrete elements. The nonlinear behaviour of the concrete was defined using the Concrete Damaged Plasticity (CDP) model based on Lubliner et. al and modified by Lee et. al [24, 25]. This considers the behaviour of the concrete after cracking as a region of plastic strain, in effect representing a continuum of micro-cracks. Additionally, account is made for the reduction in elastic stiffness as a result of damage after crushing or cracking. The uniaxial stress-strain behaviour of con-

crete in compression, after the linear elastic phase, is modelled with Equation 1 from CEB-fib [26]:

$$\sigma_c = -f_{cm}\left(\frac{k\cdot\eta-\eta^2}{1+(k-2)\cdot\eta}\right) \tag{1}$$

where $\eta = \epsilon_c/\epsilon_{c1}$, is the ratio of compression strain to crushing strain, and k is the plasticity number taken as 2.15 for C25/30 concrete. This gives a parabola shape beyond the elastic limit, with a softening effect until the ultimate limit, f_{cm}, due to compressive micro-cracks. After this point, there is a reduction in capacity as the concrete crushes. While this range is defined for completeness, the experimental programme and results from the finite element models indicate that only in the most extreme cases does the compressive strain exceed the crushing strain.

In tension, concrete is taken to be linear elastic up to its cracking stress, followed by a nonlinear tension softening model. This is described by Equation 2 from [27], where subscript t indicates tension, and ck is the cracking point occurring at a strain $\epsilon_{ck} = f_{ctm}/E_0$.

$$\sigma_t = \begin{cases} E_0\cdot\epsilon_t & for \quad \sigma_t \le f_{ctm} \\ \\ f_{ctm}\cdot\left(\frac{\epsilon_{t,ck}}{\epsilon_t}\right)^{0.4} & for \quad \sigma_t > f_{ctm} \end{cases} \tag{2}$$

The required plasticity inputs for Abaqus are given in Table 1; these definitions and the values used come from the Abaqus user manual [22]. The K_c factor is the ratio of the second stress invariant on the tensile meridian to the compressive meridian, while σ_{b0}/σ_{c0} is the ratio of initial equibiaxial compressive yield stress to initial uniaxial compressive yield stress. These values convert the uni-

Table 1: Concrete Damage Plasticity inputs

Dilation angle (ψ)	Eccentricity (m)	K_c	σ_{b0}/σ_{c0}
35°	0.1	2/3	1.16

axial stress strain relationship for compression and tension into the yield surface [28]. As the aim of a previous experiential programme [29] was to validate, rather than calibrate, the numerical model, the default values were chosen. This was confirmed by the agreement in behaviour seen in an equivalent static study [16], and the results presented below.

The steel reinforcement was modelled with circular beam elements, ID B31. The bond between the steel bars and the concrete was achieved by using Abaqus's embedded region feature, which constrains the translational degree of freedom for the reinforcement beam nodes to the interpolated values of the corresponding degrees of freedom of the surrounding concrete nodes [22]. The steel for the reinforcement was modelled with a tri-linear stress-strain relationship. Based on the tensile tests conducted on the used reinforcement, a value of 200GPa was used for Youngs Modulus and the yield stress was taken as 650MPa. An isotropic hardening law was used for the strain hardening, after yielding, up to 685MPa and 1.5% strain. Beyond this point the material was considered to be perfectly plastic. For the dynamic removal cases, the mass of the RC slab was calculated based on the assumed density and volume of the concrete and the steel. Then the additional mass to achieve the required equivalent live load was determined and added to the concrete elements and uniformly distributed across the entire slab's volume as a non-structural mass.

Initially, a gravity load was applied to all parts of the model before the support

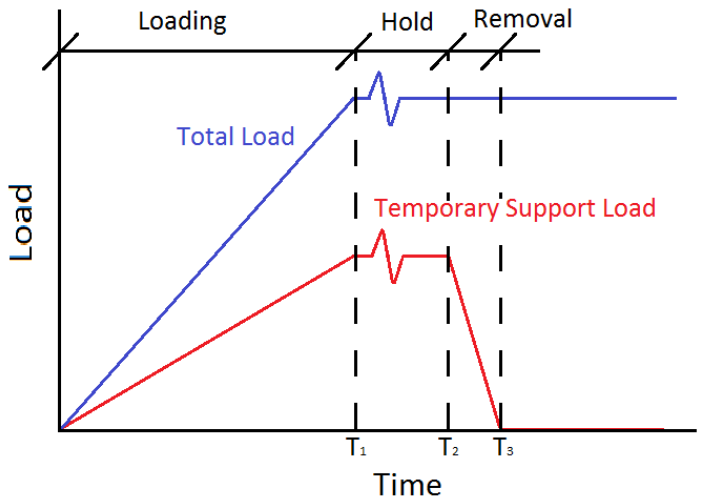

Figure 1: A schematic representation of the increase in total load and the removal of a support during dynamic tests

was removed, including the non-structural masses. This was ramped linearly at a suitable rate to prevent any inertial effects affecting the simulation at this static stage. Once the full load was reached, the loading was held constant to further ensure a static state. From this condition, the vertical reaction force from the temporary support was obtained. The fixed boundary condition was then replaced by this equivalent force and the model was ready for the removal phase.

The temporary force was then reduced from its full value to zero linearly, within the removal time period, typically 50ms. A schematic representation of the total load and the temporary support load against time is given in Figure 1, showing the linear increase in load under quasi-static conditions up to T_1, and the sudden removal of the support by linearly reducing the support load between T_2 and T_3.

To account for the increase in cracking stress due to the fast loading rates occurring during sudden events, the Model Code [26] recommends a two phase model, with the change at a strain rate of $10s^{-1}$, as shown in Equation 3.

$$(f_t/f_{ts}) = \begin{cases} (\dot{\varepsilon}_{ct}/\dot{\varepsilon}_{ct0})^{0.018} & for \quad \dot{\varepsilon}_{ct} \leq 10s^{-1} \\ \\ 0.0062\,(\dot{\varepsilon}_{ct}/\dot{\varepsilon}_{ct0})^{1/3} & for \quad \dot{\varepsilon}_{ct} > 10s^{-1} \end{cases} \tag{3}$$

where

f_t/f_{ts} = the concrete tensile DIF at $\dot{\varepsilon}$

$\dot{\varepsilon}_{ct}$ = the concrete tensile strain rate

$\dot{\varepsilon}_{ct0} = 10^{-6}s^{-1}$ (static strain rate)

As strain rates in the order of 0.01–$0.1s^{-1}$ were expected, a fixed DIF of 1.2 was applied to the cracking stress of all the concrete elements for the entire dynamic simulations. Although this overestimates the material strength, such an approach is numerically far more efficient. The reliability of this value is discussed later. No change in the material properties of the steel were made as the study did not suggest that yielding of the steel was a significant influence. Additionally, as it later discussed, the moment of maximum stress occurs at a moment of low strain rate, reducing the effect.

3. Validation against experimental results

In order to validate the FE model used in this study, experimental results from scaled slab substructure conducted by Russell et al. [29] were compared to an equivalent numerical simulation. As most aspects of the model have been previ-

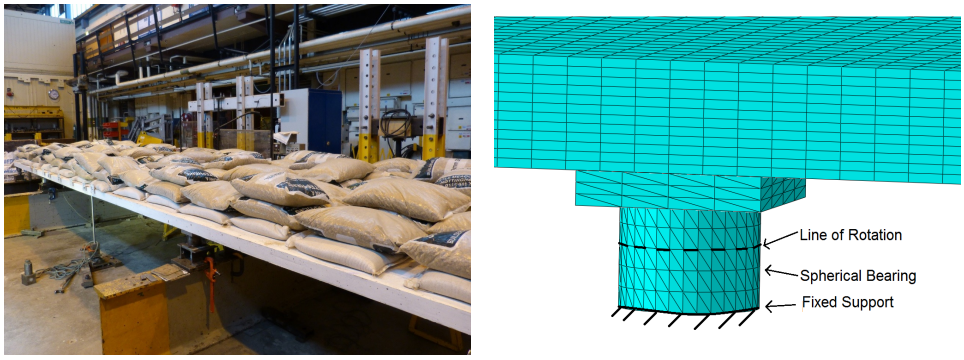

(a) Test M-D loaded (b) FE Mesh

Figure 2: Slab details

ously compared against the experimental data for static behaviour, see [16], only details relevant for a dynamic analysis of a sudden column loss are discussed here.

Two experiential scenarios are used for the validation, these are based on 1/3 scale reinforced concrete slabs. The first replicates a corner column loss, designated C-D, of a two by one bay flat slab with dimensions 4100x2100mm. The second case considers an edge column of a continuous slab by removing one of the middle supports of a 4x1 bay slab, total size 8100x2100m designated M-D, see Figure 2(a). Both slabs had a depth of 80mm. The slabs were designed to Eurocode 2 [30], with an A142 (H6@200mm) steel mesh provided for flexural reinforcement and no shear reinforcement. The supports were composed of steel plates and bearings, Figure 2(b) provides an example of the modelled support condition. One support was designed with a quick release mechanism for dynamic response analysis.

3.1. Validation of column removal time

Figure 3 shows the FE displacements results against time with different removal times compared to the experimental results. Four different times (0, 20, 50 and 100ms) are used to reduce the reaction force provided by the temporary support, as described with Figure 1. As 0ms is not possible to model computationally, the force was removed within one time step. However, the explicit analysis required a stable time increment that was typically much less than 0.1ms, which results in a practically near instantaneous removal scenario. In the test shown in Figure 3(a), there is a significant difference in the responses as the removal time changes. The first two cases, 0ms and 20ms show very similar behaviour, with peaks occurring at approximately the same time. For the 50ms removal time the peak is noticeably reduced to 79% of the instantaneous peak. Additionally, it can be seen that the peak displacement occurs later. With the 100ms case the peak is only 53% of the instantaneous removal and there is very little oscillation. Furthermore, the ratio of peak to final displacements drops from 1.59 for the instantaneous case, to 1.42 and 1.06 for 50 and 100ms respectively. This demonstrates that the modelled removal time is an important factor. By comparing the experimental results to the FE model indicates that the experimental removal time was between 50 and 100ms. However, as significant oscillations were seen in the experiment, it is likely to be closer to the 50ms value. Of final note, the experimental case reached its peak quicker than the 50ms case, despite the trend suggesting it should be longer. This may be due to the linear reduction in force at the support, which does not truly represent the motion involved in the sudden column removal.

Considering also a case with a higher super-imposed load, presented in Figure 3(b), this again shows the significant effect of removal time on the displacement

response, with longer removal times producing smaller peaks and final displacements. For this case, the peak experimental results appear to fit better with the 20ms case, although its gradient, i.e. its velocity, matches the 50ms removal very well. This is further confirmed from video footage with a high speed camera during the experimental study suggesting that the support was typically completely removed within 50ms [29]. This value is therefore a reasonable estimate of the removal time, however, towards the end of the motion, more damage occurred in the experiment than was predicted with the FE case resulting in the higher deflections.

3.2. Displacements against time

Taking the displacements against time for the corner column loss test, ID C-D, a comparison can be made between the experimental results and the FE model as shown in Figure 4. For the case with a super-imposed load of 3.0 kN/m^2, the model shows slightly higher deflections than the experiment. This is due to a lower level of stiffness, which may be due to the uncertainties in the material properties, support conditions and accuracy of the measurements. However, the difference in deflections is less than 2mm, and the damping ratio for both cases is 0.01, based on the logarithmic decrement method after the first peak. At the higher loading, 6.8 kN/m^2, the position in the middle of the adjacent bay shows a very similar relation to the experimental results, including a slight delay before moving. The peak displacements show a weaker agreement. Firstly, the numerical case shows that after the experimental case reaches equilibrium, plastic drift continues to increase the deflections in the FE model. While this phenomenon was observed in some experimental tests it did not occur in this specific specimen. Additionally, a smaller peak is predicted from the numerical case, which could either be due to the simulated support removal time being too long, or the DIF being too high for

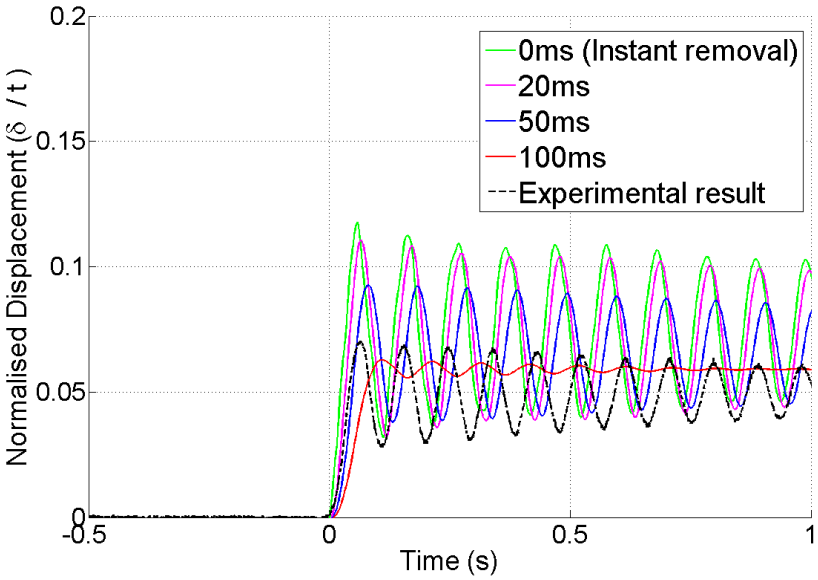

(a) 3.0kN/m^2 of loading

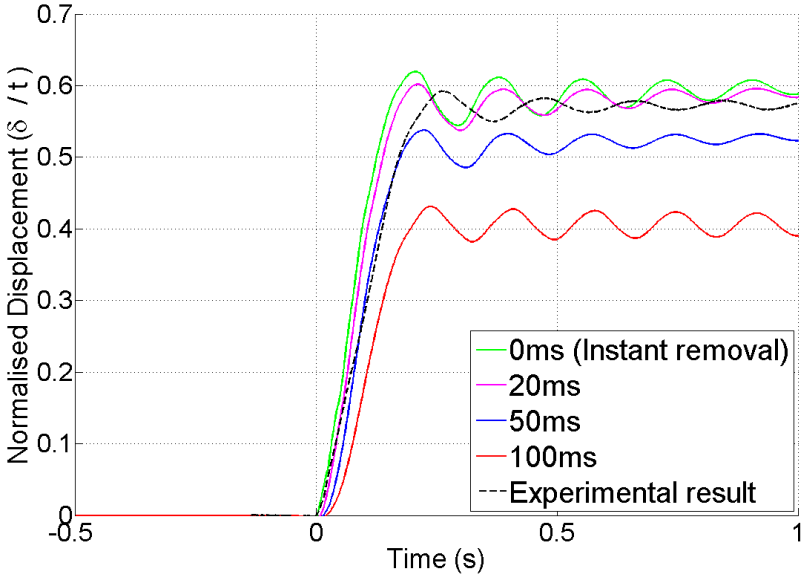

(b) 6.8kN/m^2 of loading

Figure 3: Displacements against time for different support removal times compared with experimental results - Test C-D

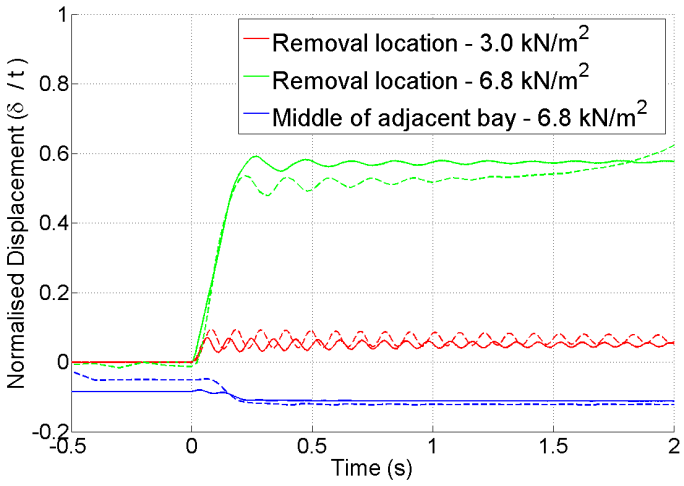

Figure 4: Normalised displacement against time for test at different locations and loadings. Experimental results (solid lines) and FE (dashed lines) are shown for test C-D (corner removal)

the strain rates.

The peak strain rate measured in the top steel over the adjacent support was $0.028s^{-1}$, which corresponds to a DIF of 1.2 according to Equation 3, the same value that was specified as a fixed increase factor. This occurred between 60 and 100ms after removal, while the peak displacement did not occur until 220ms. At the time of maximum displacement, the highest strain rate in the steel was a factor of 10 lower than the peak, which reduces the calculated concrete DIF to 1.15. This assessment indicates that the tensile concrete DIF is close to the correct value, although may still overestimate the additional capacity provided as the slab reaches its first peak. However, the difference in deflections between the numerical and experimental cases is small and is quickly damped out in both cases.

The results for the 8.1m specimen, test ID M-D, which included a continuous

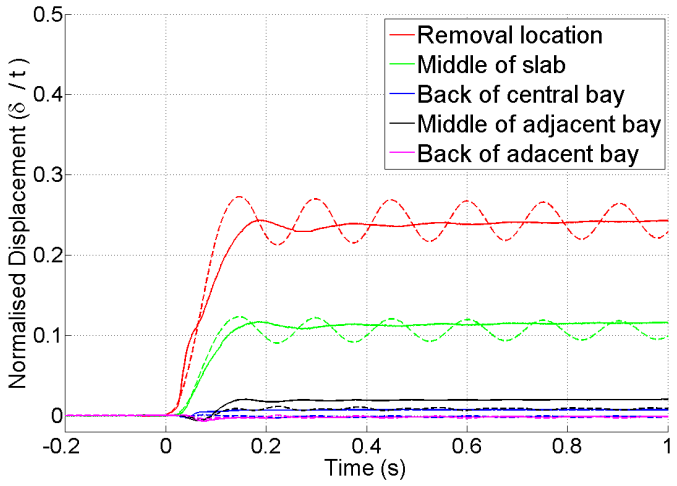

Figure 5: Displacements against time at different locations comparing experimental results (solid lines) to the FE (dashed lines) - Test M-D with 8.5 kN/m^2 of loading

slab over the adjacent supports, creating a 2x1 bay system with the middle edge column removed, are compared to the FE model in Figure 5. With a loading of 8.5 kN/m^2, the displacement values from the FE model tend towards similar values from the experimental case, in particular at the removal location, the motion is not as damped as the physical test. A clear oscillating motion can be seen from the numerical results while the experiment reached its peak more slowly with almost no oscillation. It should be noted that the other monitored locations in the adjacent bay show a better agreement, possibly as these locations experience smaller deflections and less dynamic influence.

3.3. Comparison of natural frequencies

Conducting a modal analysis of the models, to obtain the mode shapes and associated natural frequencies, allowed further validation of the models. It is ex-

pected that within the elastic range, where damage has not occurred, the frequency of oscillation corresponds closely with the 1st modal frequency. At higher loading, the extensive flexural damage and concrete cracking reduces the stiffness of the slab and therefore decreases the fundamental frequency leading to a different response from that predicted based on the initial state. The modal analysis is based on a linear perturbation and therefore nonlinear contact changes such as uplift of supports or rotation of the bearings will not be captured.

A summary of the results from the modal analysis is given in Tables 2 and 3 comparing them with the fundamental frequency of oscillation from the experimental programme and the dynamic FE tests. In both the corner and middle column removal cases, the first modal frequencies are higher than the experimental results at all loading levels. In the elastic range, the overestimation is the smallest, and is because of the issues in modelling the rotation of the supports. The frequency of oscillation of the FE model at the higher loadings shows a much better agreement to the experimental case. This suggests that the full nonlinear model provides a good representation of the reduced stiffness due to the damage and the distribution of the mass across the sample.

As the natural frequency is a function of the stiffness and the mass, by conducting a modal analysis on the initial elastic state of a structure, with a known loading, the difference in dynamic oscillation after a sudden column loss is due to the reduction in stiffness as a result of damage.

4. Description of numerical parameter study

The validated FE model was extended to investigate the influence of changing parameters on the response of typical flat slab structures after a column loss event.

Table 2: Comparison of the frequencies from a modal analysis and the dominant frequency observed in the experimental and FE results - Test C-D

Loading	1st Mode (Hz)			2nd Mode (Hz)
	Experiment	FE		FE
(kN/m^2)	Displacements	Displacements	Modal	Modal
3.0	11.0	9.76	13.6	30.5
6.8	5.41	5.68	9.05	20.2
7.7	3.54	N/A	8.53	19.1

Table 3: Comparison of the frequencies from a modal analysis and the dominant frequency observed in the experimental and FE results - Test M-D

Loading	1st Mode (Hz)			2nd Mode (Hz)
	Experiment	FE		FE
(kN/m^2)	Displacements	Displacements	Modal	Modal
3.1	13.4	11.1	15.1	30.1
6.9	8.6	7.78	10.1	20.1
8.5	6.0	6.64	9.1	17.9

The plan and elevation of the floor model is shown in Figure 6(a). $L_{over} = 500mm$, $c = 400mm$ and $H = 3000mm$ are the overhang, column width and storey height respectively, kept constant for all models. As solid elements were used, the columns are rigidly connected to the slab at all shared nodes across their cross section. The span length, L, and the slab thickness, t, were varied from 4 to 6m and 180 to 250mm respectively. Further information of the model can be obtained from reference [16].

Each of the models was designed to meet current Eurocode requirements according to EN 1992 [30]. Characteristic dead loading was based on the selfweight of the material plus an additional 1.0kN/m^2 to account for other finishes. Live loading for design was taken at 2.5kN/m^2. Unless otherwise stated, the characteristic compressive concrete strength was 30MPa. Based on the design forces, adequate flexural steel was provided, including the requirement to place 50% of the tensile steel for hogging moments within 0.125 times the span width. In all locations, for both top and bottom steel, at least a minimum area of steel according to EC2 was provided, typically H10 bars at 300mm centres. To meet durability specifications, 25mm of cover was provided to all steel. Each designed model configuration met the required shear stress capacity for punching shear without the inclusion of shear reinforcement.

In total, five different arrangements were considered as listed in Table 4. The span to depth ratios are based on the effective span length, L_{eff}, of an internal bay with a continuous slab over the supports.

For the column removal simulation, a uniformly distributed load was applied for an accidental load case, w_{ac}, as given in Equation 4 from US General Services

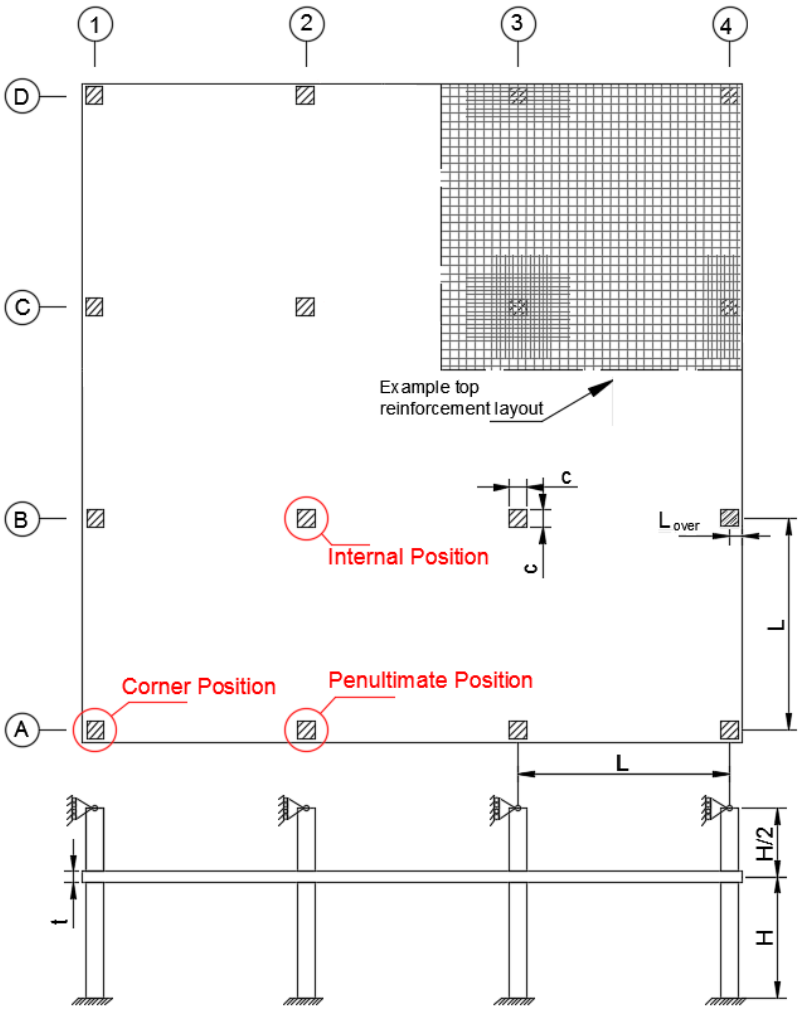

(a) Plan and elevation

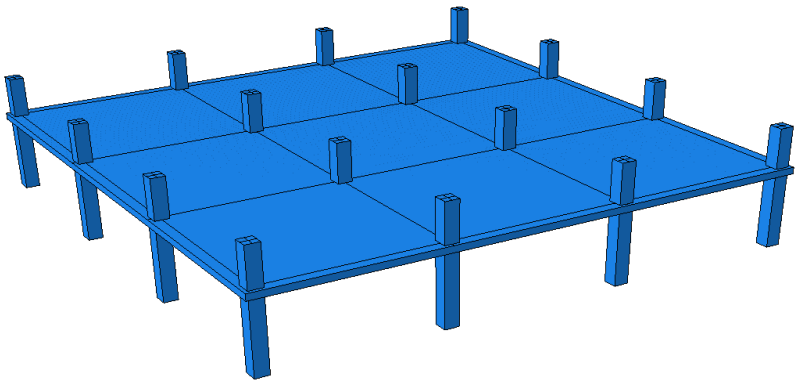

(b) Rendering of finite elment floor model

Figure 6: Floor model layout for numerical study

Table 4: Span length and slab thickness for each model

Span length L (mm)	Slab thickness t (mm)	Effective span L_{eff}	Span to depth ratio L_{eff}/t
4000	180	3780	21.0
4000	250	3850	15.4
5000	200	4800	24.0
5000	250	4850	19.4
6000	250	5850	23.4

Administration (GSA) [1]:

$$w_{ac} = 1.2DL + 0.5LL \tag{4}$$

where DL and LL are the Dead and Live Loads respectively, representing one of the highest commonly used design load factors.

The Dynamic Amplification Factor (DAF), that is the required increase in applied force for a static analysis to represent the inertial effects from a dynamic case, can be determined by comparing the results from the two simulations. The DAF can be calculated by taking the peak displacement from the dynamic analysis and finding what force factor is needed on a nonlinear static model to achieve the same displacement. This approach is suitable for attempts to correlate flexural damage between static and dynamic analyses, which is related to the deflection response. However, the shear force increase is not directly related to the measured deflections. Therefore, a DAF based on the peak reaction force occurring at a column, compared to the static increase condition will be also considered in this study.

5. Numerical results and discussion

5.1. Dynamic displacement for different span to depth ratios

Figure 7 shows the normalised displacements against time for models with different span to depth ratios. The removed column locations are shown in Figure 6(a), for the two column removal case the corner and penultimate column locations were chosen. The key displacement results are also presented in Table 5 from all the models. Note that due to the high computational cost in running these simulations, later analyses were terminated earlier, once patterns had been established, to ensure responsible use of resources. The results are also normalised against the ductility factor, μ_δ, defined from Equation 5.

$$\mu_\delta = \frac{\delta}{\delta_y} \tag{5}$$

where δ and δ_y are the displacement and the static yield displacement of the removal point respectively. A bilinear relationship of the static displacement against load was applied to get the yield displacement for each scenario, whilst ensuring the ensure the area under the simplified model is equal to the area under the measured curve [16].

In general, increasing L_{eff}/t leads to larger normalised deflections, although exceptions occur due to the influence of the higher selfweight that comes with thicker slabs, which explains why larger displacements are seen for the 24.0 case compared to 23.4 for the internal removal scenario.

In all the cases, while the deflections as a function of the depth remained low, less than 0.159 times the thickness of the slab for a single column loss, the level of nonlinearity demonstrated that the structure may be stressed beyond its elastic limit, by up to 3.31 times δ_y in the highest case. Additionally, removing two

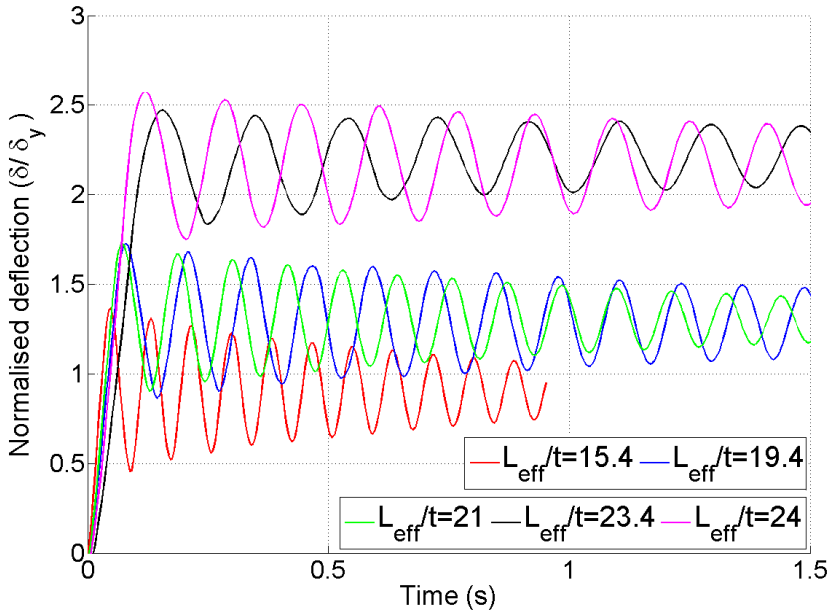

(a) Corner column removal

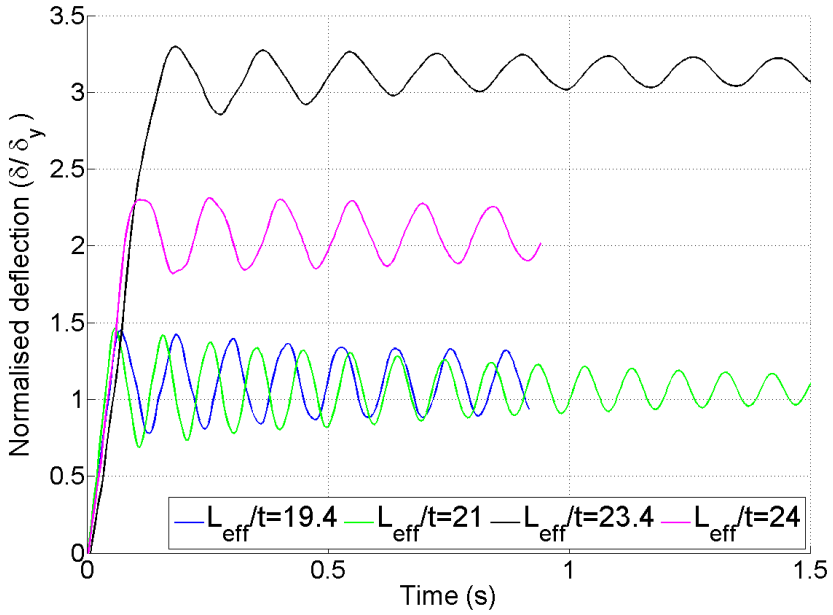

(b) Internal column removal

Figure 7: Normalised displacement against time for different span to depth ratios

columns naturally creates a larger displacement response, with a higher δ_{max}/δ_y ratio, although δ_{max}/t is still only 0.283. This suggests that although material nonlinearity may occur, the slab has not deformed enough for the effects of geometric nonlinearity to be dominant.

A further comparison is given in Table 6, which shows the frequency and damping values for the models. In each case, the frequency of oscillation is slightly lower than the value obtained from the modal analysis. This is due to the reduction in stiffness of the concrete elements as a result of damage. However, this change is not typically very large, indicating that the system is close to elastic. Similarly, the damping ratio is typically under 2% from the model's free decay period, suggesting the damage sustained has not affected the response of the structure significantly.

A comparison of the displacements against time for the four removal scenarios is given in Figure 8 for slabs with L_{eff}/t = 19.4. From these results all the single column loss events show a similar level of normalised displacement, with the corner case slightly higher than the others. When two columns are removed, significantly higher deflections occur, although the frequency of the oscillations is smaller, as also shown in Table 6.

5.2. Displacement response for different removal times

The previous results were all based on an assumed instantaneous column removal, commonly used for scenario independent analysis. In reality it may take longer for the support to be completely removed. Changing this removal time changes the dynamic response of the structure, as can be seen in Figure 9. For the corner column removal, Figure 9(a), a longer removal time results in a smaller and later peak displacement for all cases. It can be noted that up to 20ms, all

Table 5: Summary of dynamic displacements

Removal location	Span to depth ratio, L_{eff}/t	Max displacement	
		δ_{max}/t	δ_{max}/δ_y
Corner	15.4	0.018	1.37
	19.4	0.051	1.73
	21.0	0.055	1.73
	23.4	0.159	2.47
	24.0	0.123	2.58
Internal	19.4	0.040	1.45
	21.0	0.041	1.46
	23.4	0.156	3.31
	24.0	0.098	2.31
Penultimate	19.4	0.046	1.55
Two Edge	19.4	0.283	4.58

Table 6: Summary of dynamic values from the displacement response

Removal location	Span to depth ratio, L_{eff}/t	Modal frequency (Hz)	Displacement frequency (Hz)	Damping ratio
Corner	15.4	11.96	11.85	0.014
	19.4	7.96	7.78	0.012
	21.0	8.94	8.71	0.016
	23.4	5.64	5.23	0.011
	24.0	6.51	6.19	0.011
Internal	19.4	9.01	8.75	0.012
	21.0	10.46	10.0	0.020
	23.4	7.45	5.63	0.010
Penultimate	19.4	8.74	7.62	0.016
Two Edge	19.4	5.44	4.90	0.026

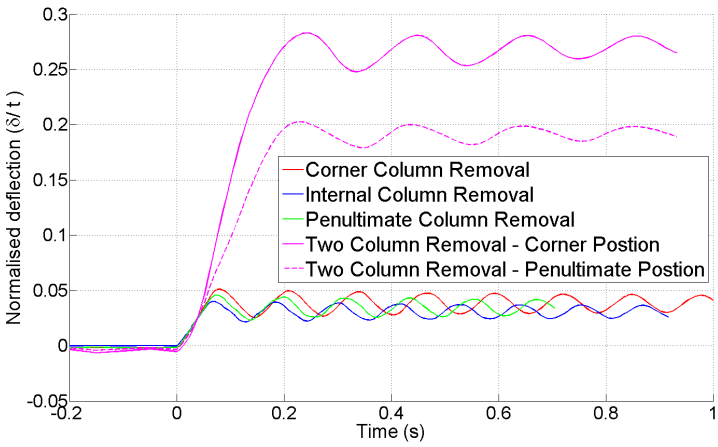

Figure 8: Normalised displacement against time for different column loss scenarios. $L_{eff}/t = 19.4$

the results are very similar indicating the removal time does not play a significant role in this range. However, the response is noticeably different for the cases with longer removal times. Furthermore, for the 250ms case it can be seen that the removal is so slow that it interrupts the motion of the slab. The internal column removal, Figures 9(b) and 9(c), shows a similar behaviour. The displacements from the static analysis are also plotted with the dashed line, demonstrating that as the removal time is increased, the response tends towards the quasi-static. However, even at the longest times considered, the dynamic effects are still evident. Additionally, the nonlinearity in the dynamic response can be seen with nearly all cases exceeding the yield displacement.

5.3. Reaction forces against time

Similar to the static case, reaction forces at the bases of all columns were monitored after the column loss event to provide an indication into the increase in axial force at those locations. As punching shear failure, rather than column

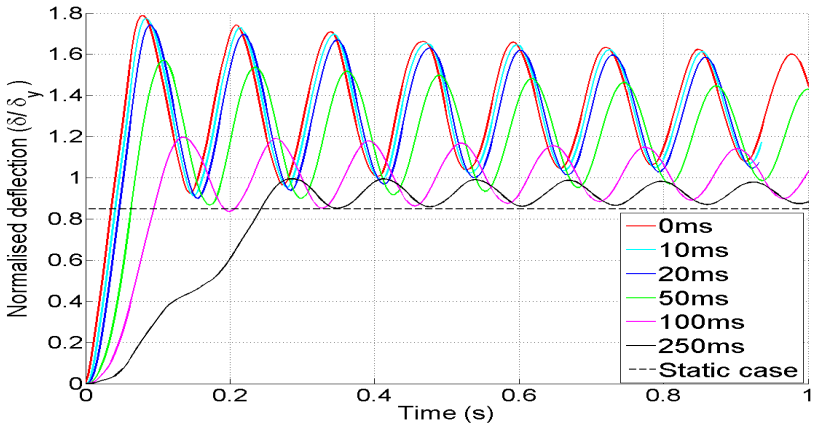

(a) Corner column removal: L_{eff}/t=19.4

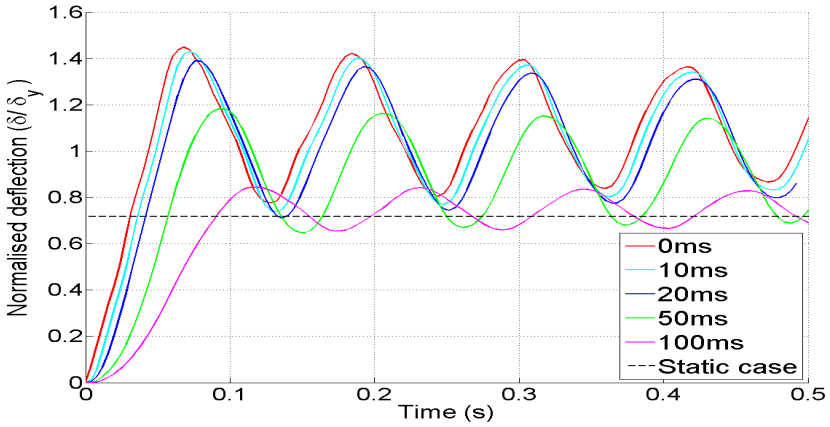

(b) Internal column removal: L_{eff}/t=19.4

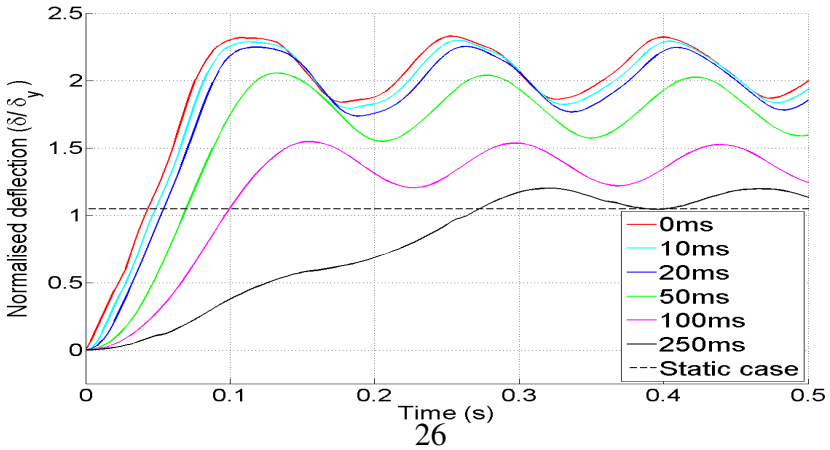

(c) Internal column removal: L_{eff}/t=24

Figure 9: Normalised displacement against time for different removal times

failure, is a major concern for progressive collapse of flat slabs, shear demand will also be considered. Figure 10 shows the change in reaction forces at four remaining columns after a corner column is lost. Also the maximum displacement with time is plotted to allow comparison between the responses. The immediately adjacent column, A2, shows the largest increase in loading, with other locations, such a A3, experiencing a decrease. It can also be seen that the force-time response for the critical column matches the displacement response. That implies that the highest shear forces are transmitted through the column at the moment the slab reaches its temporary static condition. The forces in the other columns oscillate at a higher frequency, indicating that higher modes are involved. This is to be expected as reaction forces are related to the acceleration of the slab, which emphasises higher frequency components of the motion. However, the amplitude are much smaller than the closest columns, demonstrating this is only a minor effect.

Figure 11 shows the dynamic removal of an internal column. After column B2 is removed, A2 and B3 experience the highest increase in column reaction force. Considering the penultimate column loss in Figure 12, it can be seen that the 3 orthogonally adjacent columns show very similar responses. In this case the corner column, A1, undergoes the largest change from the fully supported condition. This plot also shows the response of Column B3, a support diagonally across the bay from the removal location. The relative load here oscillates around a value close to 100%, indicating that the dynamic motion of the slab influences this location. Therefore, there is a slight increase in loading to these areas after a sudden column loss event, even though the static analysis predicted it would reduce. Again, forces in remote columns oscillate at a higher frequency.

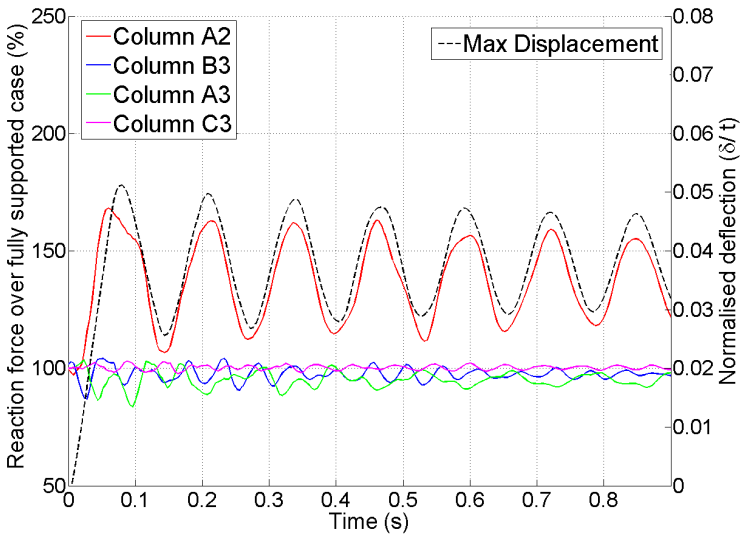

Figure 10: Change in column reaction forces against time. Corner column removal. L_{eff}/t=19.4

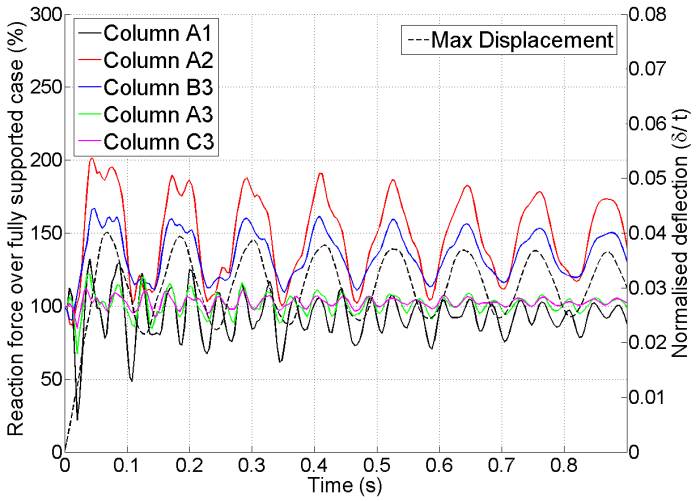

Figure 11: Change in column reaction forces and maximum displacement against time . Internal column removal. L_{eff}/t=19.4

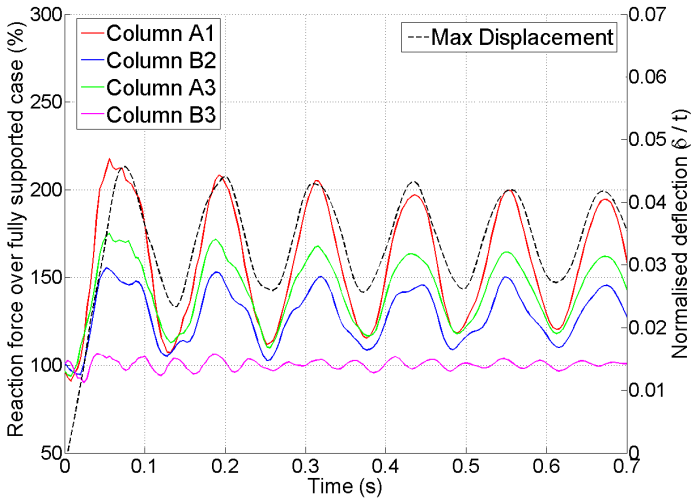

Figure 12: Change in column reaction forces and maximum displacement against time. Penultimate column removal. L_{eff}/t=19.4

For a sudden removal of two columns, Figure 13 provides the reaction response. Although the dominant frequency and behaviour follows the peak displacement of the slab in this case, it is clear that other frequencies also play a role in the response as a consequence of a larger portion of the structure being involved in the motion.

Finally, the influence of the removal time on the reaction forces is shown in Figure 14 for a corner and internal column loss. As with the displacement results shown previously, increasing the removal time results in a lower and later peak.

5.4. Punching shear assessment

Although each simulation was run excluding shear failure, the punching shear capacity of the unreinforced flat slab connections can be estimated with the Critical Shear Crack Theory (CSCT) developed by Muttoni [31]. The CSCT has been

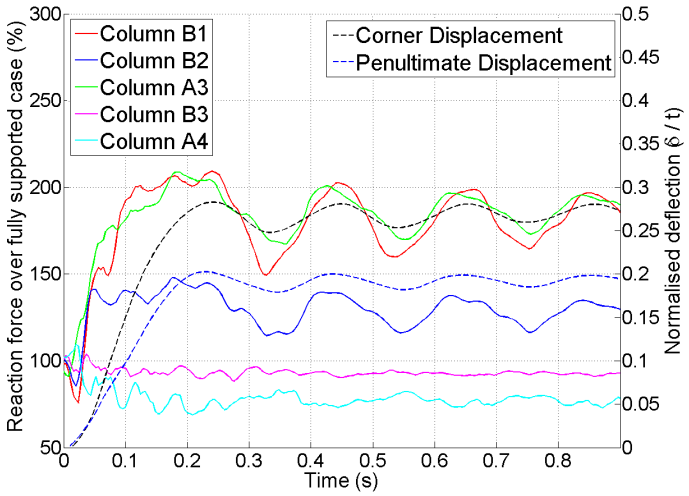

Figure 13: Change in column reaction forces and maximum displacement against time. Two column removal. L_{eff}/t=19.4

demonstrated to be suitable for assessing progressive collapse of flat slab structures [20, 32]. Additionally, it was previously used to consider the potential for shear failure during a static analysis of a column loss scenario for the same parameters presented here [16]. The CSCT theory assumes that shear capacity of a slab column connection reduces with increasing rotation of the slab, and therefore is related to the maximum displacement.

From the equivalent static analysis it was shown that the internal column loss event with the largest span-to-depth ratio was most susceptible to punching shear failure. However, as in most scenarios the structure did not undergo large deformations and the connection rotations remained relatively small, typically below 0.005 radians. The result of this is that even with the larger shear forces transmitted through the column due to the dynamic effects, punching shear failure was not

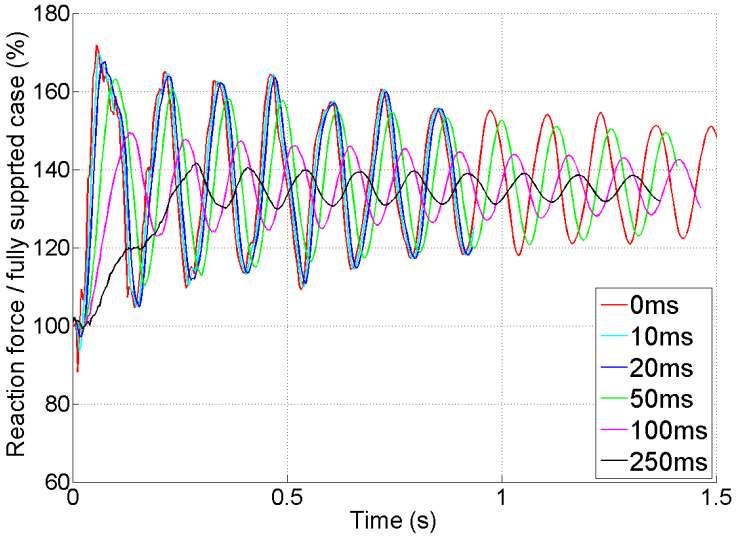

(a) Corner column loss. Reactions at Column B2

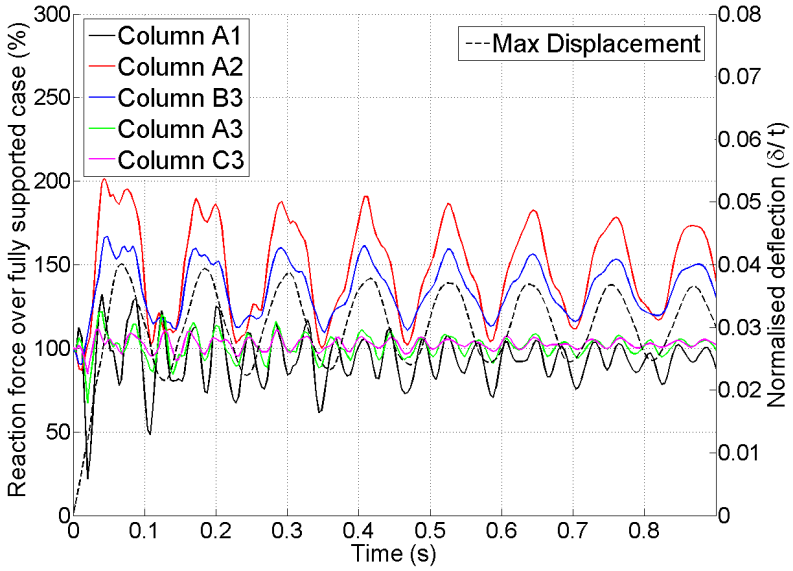

(b) Internal column removal. Reactions at Column B3

Figure 14: Change in column reaction forces against time for different removal times. L_{eff}/t=19.4

a concern for any of the cases considered.

5.5. Influence of strain rate effects

A final consideration was given to the strain rates in the steel reinforcement after a column loss. Figure 15 shows the maximum strain rate against time for the top flexural reinforcement after a corner column is removed, for models with different span to depth ratios. Also plotted is the displacement against time to allow further comparisons. It can be seen that the maximum strain rate in the steel reinforcement does not occur at the time of highest displacement and therefore stress. Instead it reaches its peak whilst the slab is moving towards its first peak. The strain rate in the steel reinforcement during the subsequent oscillations is significantly smaller than the initial peak. Additionally, structures with larger span to depth ratios in general result in higher strain rates, primarily because higher deflections occur within the short time period. However, the case with the highest span to depth ratio, L_{eff}/t = 24.0, shows very similar peak values to the 19.4 case, despite higher deflections. This suggests that even if more of the structure is damaged, an individual section of steel reinforcement will not always experience higher strain rates.

The peak strain rate values from Figure 15 are 0.023 and 0.043s^{-1} for L_{eff}/t values equal to 15.4 and 24.0 respectively. Based on Equation 3 this corresponds to a DIF for the concrete of 1.20 and 1.21 for the two cases. This small variation suggests that, for the range and conditions for normal structures, the DIF for concrete is around 1.20 at its most critical, and much lower past the initial peak.

With this value for the increase in tensile strength for concrete, comparisons were made to determine its significance. Figure 16 plots the maximum strain rates for models with different concrete strengths. For the higher grade concrete,

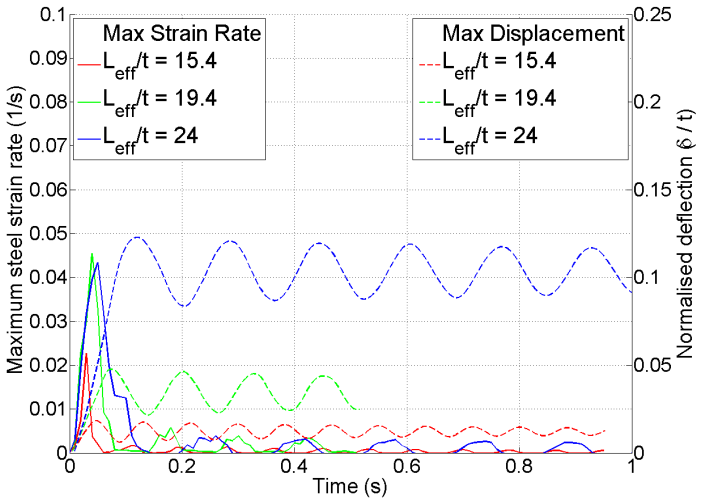

Figure 15: Maximum steel strain rate against time after corner column loss for different models. Also showing peak displacements against time.

increasing the tensile strength further due to dynamic effects, does not change the maximum strain rate with both cases peaking at 0.045s^{-1}. For the f_{ck} =20MPa case, applying a DIF does change the strain rate response. Although the peaks are almost identical, 0.042 and 0.043s^{-1} respectively for with and without the DIF applied, the case with the higher tensile strength shows a later, and narrower, peak as a result of less damage occurring.

The effect of applying a DIF to the model can be seen in Figure 17, which compares the normalised displacement against time. As the span to depth ratio is increased, the effect of the higher tensile capacity, due to strain rates, becomes more noticeable. This is logical as these cases have already been shown to experience more flexural damage and therefore increasing the capacity will improve this response. However, the maximum difference observed here is still less than

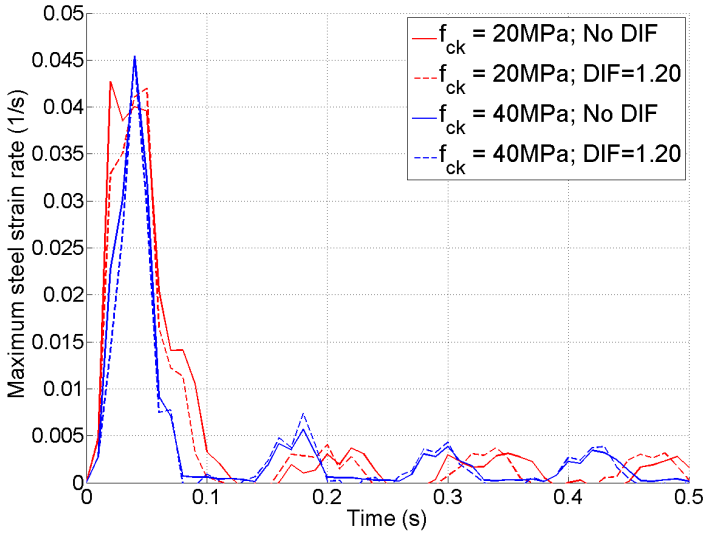

Figure 16: Maximum steel strain rate against time after corner column loss $L_{eff}/t = 19.4$

8mm, or 3% of the slab depth. Structures that experience higher deflections due to their material or geometric properties benefit more from the additional capacity, although these results suggest it this is not a major effect. Also note that, as the increase in concrete strength was applied to the entire model for the whole analysis, these plots represent the maximum possible change due to the DIF. In reality the response will be closer to the condition with no material strength increase.

Figure 18 shows the maximum strain rates for an internal column loss. This case affects more of the structure and includes the response of the bottom steel under sagging conditions. Again that the peak strain rates occur before the first displacement peak, and after this point are an order of magnitude smaller. Comparing the response of the top and bottom steel shows the peaks are 0.055 and $0.071 s^{-1}$ respectively. This corresponds to a concrete DIF of 1.22 for both cases.

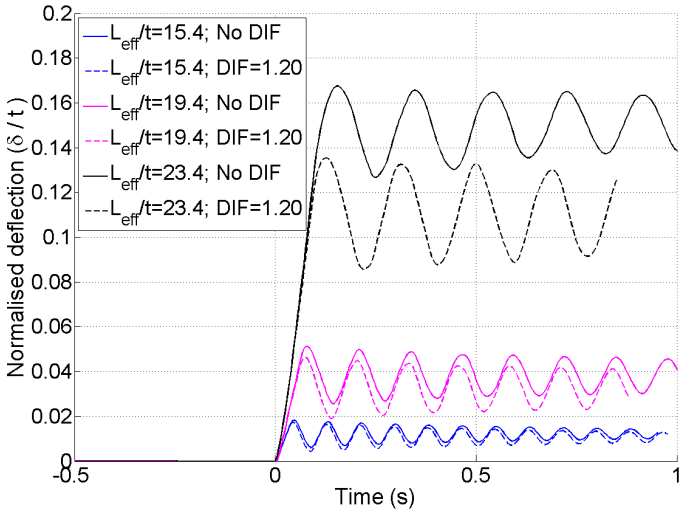

Figure 17: Normalised displacement against time after corner column loss comparing effect of applying a DIF

The bottom steel peaks occur after the top steel. This is due to the slab changing from a hogging to a sagging condition after the column is removed, therefore cracking does not occur in this area until later. Of final note is the location of the maximum strain rates in the top steel. The most critical area is over supports that are at the edge of the structure, i.e. B1 and A2. However, when these areas are excluded, the internal columns still undergo strains at a rate of up to $0.043s^{-1}$.

6. Static to dynamic comparison

As both static push down tests with an additional force factor and dynamic removal simulations have been conducted on the same models, comparisons can be made to determine the influence of dynamic effects, especially the Dynamic Amplification Factor (DAF). Figure 19 compares the displacement at the column

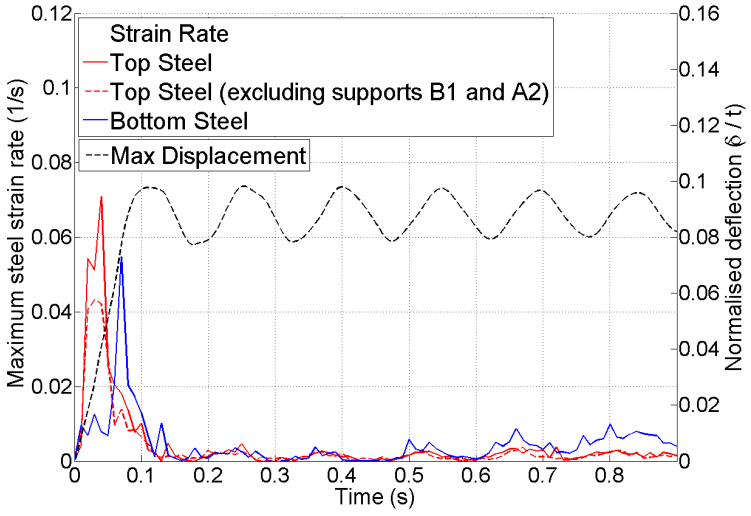

Figure 18: Maximum steel strain rate against time after an internal column loss. $L_{eff}/t = 24$

removal location for the different conditions. The DAF is taken as the load factor applied to the bays around the removed column, which results in the same displacement as the peak dynamic result. For the range of structures modelled, the DAF varies between 1.39 and 1.62. There is a linear relationship shown with increasing span to depth ratio of the slab linked with a smaller DAF. However, when just one removal scenario is considered the trend becomes much stronger, for example for a corner column loss R^2=0.947. Additionally, by extrapolating beyond the data it can be seen that as the structure becomes stiffer the DAF tends towards 1.97. This suggests that the influence of inertia is not directly related to the span to depth ratio of the structure, but rather the extent of damage, and therefore nonlinearity in the force displacement response. For a purely elastic single degree of freedom system, with no damping, a DAF of 2 is expected. However, as structures within the normal design range undergo nonlinear behaviour, the DAF

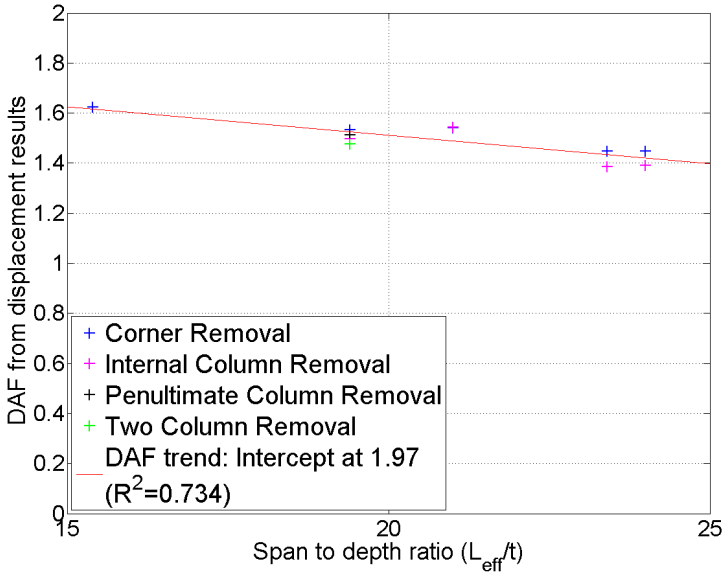

Figure 19: DAF from displacement values for different span to depth ratios

can be reduced accordingly.

A similar comparison can be made based on the maximum column reaction forces. Standard approaches for the DAF assume that the loading on the surrounding supports is increased by the same factor as for displacement predictions (see for example GSA guidelines [1]). However, as reaction forces are less influenced by nonlinear effects, such approaches may not be appropriate. Figure 20 shows the required DAF to create the same static forces in the critical surrounding columns as caused by the peak dynamic case. As with the displacement values, the amplification factor is calculated for different span to depth ratios. For the corner loss condition, with column A1 removed, the reaction based DAF is given in Figure 20(a). It is shown that there is a linear relationship against the span to depth ratio (R^2=0.789), and the DAF ranges between 1.38 and 1.43 for usual

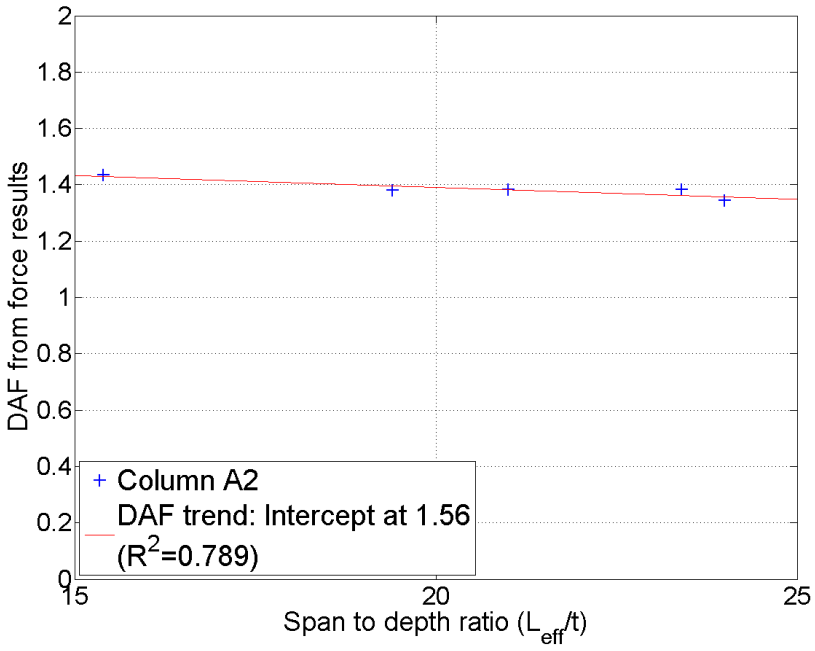

(a) Corner column removal scenario

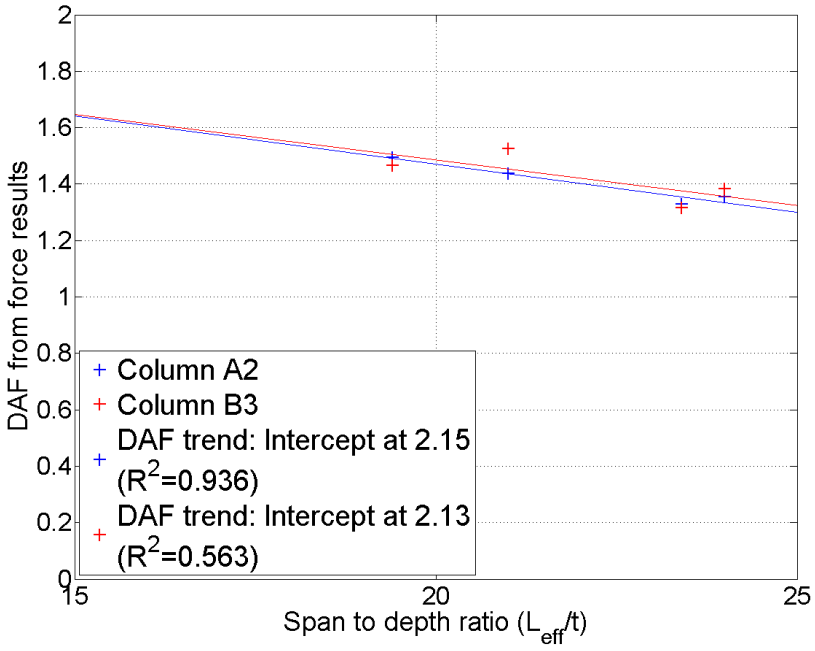

(b) Internal column removal scenario

Figure 20: DAF from reaction forces for different span to depth ratios

structural arrangements. Considering the internal column removal, shows that the two most critical remaining columns have very similar trend lines, although column B3 has a much weaker agreement based on its R^2 value. In this case the DAF varies between 1.31 and 1.53. However, when these trends are extrapolated for stiffer structures, they reach maximum values of 2.13 and 2.15, as shown by the intercept marked on Figure 20(b). This may indicate that for structures with very short spans, the distribution of loads to surrounding columns changes from the typical bending profile.

The results discussed before indicated that increasing the removal time for the column decreases the influence of the dynamic effects. Therefore, a modification to the DAF can be applied to consider the effect of removal time, which is defined as the ratio of the DAF from instantaneous removal to the DAF calculated from the slower period. Figure 21 plots this factor against a normalised removal time, based on the fundamental period of floor section with elastic properties. The nature of this reduction factor means that as the value reaches 1, the response matches that of an instantaneous removal. Additionally, the lowest value would be 0.5, corresponding to an undamped elastic system with very slow column removal to minimise inertial effects. For the range of conditions presented, if the support is removed within 10% of the fundamental period, the reduction factor is above 0.995. Similarly, at 20% of the fundamental period, the factor exceeds 0.975. However, if we take the corner case, with removal time of 80% of the fundamental period, the DAF is reduced to 1.21, demonstrating inertial effects may still be significant. At the longest case considered, twice the fundamental period, the DAF reduced to 1.10, which indicated that the dynamic effects are not removed entirely even in very slow column removal scenarios. When using scenario-independent

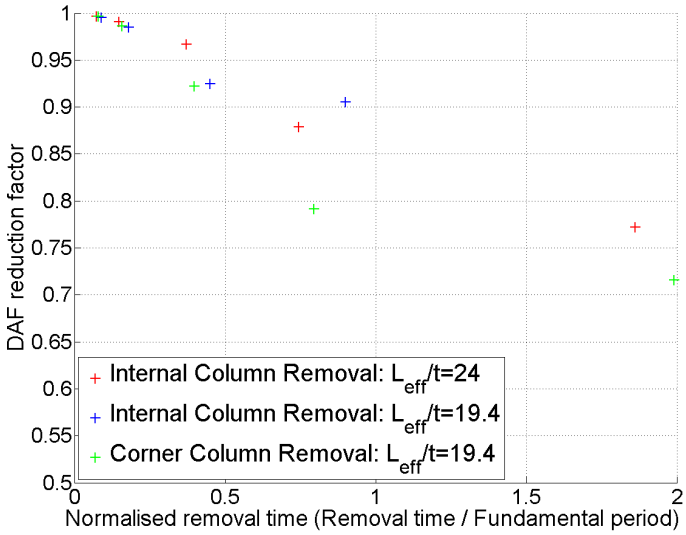

Figure 21: Reduction in DAF from displacement values due to column removal time

analysis approaches in design it is still recommended to assume instantaneous removal.

7. Summary and conclusions

This study applied an experimentally validated finite element model to consider the response of a Reinforced Concrete (RC) flat slab structure after different column loss scenarios, focusing on the dynamic issues involved. By varying material and geometric factors and comparing to equivalent static cases the influence of the dynamic effects, such as force amplification and material strength increase due to strain rate effects, were considered.

The dynamic response of RC flat slab structures after a column loss demonstrates that a sudden removal can considerably increase the peak displacements

and the shear forces compared to the static condition. The DAF for displacement values is related to the extent of damage and nonlinearity within the force displacement response. The DAFs calculated for all flat slabs considered in this study were between 1.39 and 1.62. Similar amplification factors were measured for the reaction forces (1.31–1.53), with peak shear forces exceeding 200% of the fully supported condition. These results are in line with previously presented results for beam systems, however, the redistribution of forces is naturally more complicated for due to the RC slab behaviour. Although these values are less than the 2.0 factor commonly used in design, it is clear that a good understanding of the failure mechanisms and redistribution of forces for the structure is required if lower values are used.

Additionally, the results demonstrated that removing a column more slowly results in smaller peak deflections. This can be compared to the natural period of the elastic floor section. If the support is removed within 10% of the period of the floor, the dynamic response is almost identical to the instantaneous condition. As this time increases, the equivalent DAF also decreases, however, even at a time length of twice the natural period, dynamic effects still play a considerable role, indicating that to achieve the static removal scenario requires a much slower case.

Finally, although the sudden removal, and the related strain rates, change the material properties, their influence is limited. Based on the measured strain rates in the steel reinforcement, the peak concrete DIF was around 1.20. However, this value is only relevant in limited areas and for a short period of time. Furthermore, comparing the effect of increasing the tensile capacity of the concrete, demonstrates that such an increases does not significantly change the response of the structure, as also seen with 2D frame structures [13, 14]. This is partly due to

the fact that, for the range of slabs considered in this study, the concrete was not stressed far beyond its elastic limits in most cases. Exceptions for this may occur with low strength concrete, or very severe damaging events such as multiple column loss.

Acknowledgements

The authors would like to acknowledge the Early Career Research and Knowledge Transfer grant awarded by the University of Nottingham to Dr. Hajirasouliha that funded the project. They are also are grateful for access to the University of Nottingham High Performance Computing Facility, on which the simulations were run.

References

[1] GSA (General Services Administration), Alternate path analysis & design guidelines for progressive collapse resistance, General Services Administration (2016).

[2] DoD, Unified facilities criteria: design of buildings to resist progressive collapse, Technical Report, UFC 4-023-03. United States Department of Defense, 2009.

[3] HM Government, Building Regulations 2000. Approved Document A, 2010.

[4] A. J. Pretlove, M. Ramsden, A. G. Atkins, Dynamic Effects in Progressive Failure of Structures, International Journal of Impact Engineering 11 (1991) 539–546.

[5] P. Ruth, K. A. Marchand, E. B. Williamson, Static equivalency in progressive collapse alternate path analysis: Reducing conservatism while retaining structural integrity, Journal of Performance of Constructed Facilities 20 (2006) 349–364.

[6] M. H. Tsai, B. H. Lin, Dynamic Amplification Factor for Progressive Collapse Resistance Analysis of an RC Building, Structural Design of Tall and Special Buildings 18 (2009) 539–557.

[7] B. S. Iribarren, P. Berke, P. Bouillard, J. Vantomme, T. J. Massart, Investigation of the influence of design and material parameters in the progressive collapse analysis of RC structures, Engineering Structures 33 (2011) 2805–2820.

[8] A. Naji, F. Irani, Progressive collapse analysis of steel frames: Simplified procedure and explicit expression for dynamic increase factor, International Journal of Steel Structures 12 (2012) 537–549.

[9] A. McKay, K. Marchand, M. Diaz, Alternate path method in progressive collapse analysis: Variation of dynamic and nonlinear load increase factors, Practice Periodical on Structural Design and Construction 17 (2012) 152–160.

[10] J. Yu, T. Rinder, A. Stolz, K. Tan, W. Riedel, Dynamic Progressive Collapse of an RC Assemblage Induced by Contact Detonation, Journal of Structural Engineering 140 (2014) 04014014.

[11] M. Sasani, A. Kazemi, S. Sagiroglu, S. Forest, Progressive Collapse Resis-

tance of an Actual 11-Story Structure Subjected to Severe Initial Damage, Journal of Structural Engineering-ASCE 137 (2011) 893–902.

[12] E. Livingston, M. Sasani, M. Bazan, S. Sagiroglu, Progressive collapse resistance of RC beams, Engineering Structures 95 (2015) 61–70.

[13] A. T. Pham, K. H. Tan, Experimental study on dynamic responses of reinforced concrete frames under sudden column removal applying concentrated loading, Engineering Structures 139 (2017) 31–45.

[14] A. T. Pham, K. H. Tan, Static and Dynamic Responses of Reinforced Concrete Structures under Sudden Column Removal Scenario Subjected to Distributed Loading, Journal of Structural Engineering 145 (2018) 04018235.

[15] L. Keyvani, M. Sasani, Y. Mirzaei, Compressive membrane action in progressive collapse resistance of RC flat plates, Engineering Structures 59 (2014) 554–564.

[16] J. M. Russell, J. S. Owen, I. Hajirasouliha, Nonlinear behaviour of reinforced concrete flat slabs after a column loss event, Advances in Structural Engineering (2018).

[17] Y. Mirzaei, M. Sasani, Progressive collapse resistance of flat slabs: modeling post-punching behavior, Computers and Concrete 12 (2013) 351–375.

[18] P. Olmati, J. Sagaseta, D. Cormie, A. Jones, Simplified reliability analysis of punching in reinforced concrete flat slab buildings under accidental actions, Engineering Structures 130 (2017) 83–98.

[19] K. Qian, B. Li, Performance of Three-Dimensional Reinforced Concrete Beam-Column Substructures under Loss of a Corner Column Scenario, Journal of Structural Engineering-ASCE 139 (2013) 584–594.

[20] J. Liu, Y. Tian, S. L. Orton, Resistance of flat-plate buildings against progressive collapse. ii: system response, Journal of Structural Engineering 141 (2015) 04015054.

[21] L. J. Malvar, C. A. Ross, Review of strain rate effects for concrete in tension, ACI Materials Journal 95 (1998) 735–739.

[22] Simulia, ABAQUS Inc. User Manuel, version 6.10, 2010.

[23] A. S. Genikomsou, M. A. Polak, 3d finite element investigation of the compressive membrane action effect in reinforced concrete flat slabs, Engineering Structures 136 (2017) 233–244.

[24] J. Lubliner, J. Oliver, S. Oller, E. Onate, A Plastic-Damage Model for Concrete, International Journal of Solids and Structures 25 (1989) 299–326.

[25] J. H. Lee, G. L. Fenves, Plastic-damage model for cyclic loading of concrete structures, Journal of Engineering Mechanics-ASCE 124 (1998) 892–900.

[26] Fédération Internationale du Béton, Model code 2010 : final draft, Bulletin / Federation Internationale du Beton ; 65-66, International Federation for Structural Concrete (fib), 2012. Prepared by fib Special Activity Group 5, New Model Code.

[27] H. Okamura, K. Maekawa, Nonlinear-Analysis and Constitutive Models of

Reinforced-Concrete, Computer Aided Analysis and Design of Concrete Structures, Vols 1 and 2 (1990) 831–850.

[28] T. Jankowiak, T. Lodygowski, Identification of parameters of concrete damage pasticity constitutive model, Foundations of Civil and Enviromental Engineering (2005) 53–69.

[29] J. Russell, J. Owen, I. Hajirasouliha, Experimental investigation on the dynamic response of RC flat slabs after a sudden column loss, Engineering Structures 99 (2015) 28–41.

[30] EN 1992, BS EN 1992: Eurocode 2 - Design of concrete structures - Part 1-1: General rules and rules for buildings, 2004.

[31] A. Muttoni, Punching shear strength of reinforced concrete slabs without transverse reinforcement, ACI Structural Journal 105 (2008) 440–450.

[32] K. Micallef, J. Sagaseta, M. F. Ruiz, A. Muttoni, Assessing punching shear failure in reinforced concrete flat slabs subjected to localised impact loading, International Journal of Impact Engineering 71 (2014) 17–33.